Journal of Nuclear Materials 415 (2011) 84–95

Contents lists available at ScienceDirect

Journal of Nuclear Materials

journal homepage: www.elsevier.com/locate/jnucmat

Stochastic cluster dynamics method for simulations of multispecies irradiation damage accumulation

Jaime Marian *, Vasily V. Bulatov

Lawrence Livermore National Laboratory, Livermore, CA 94551, United States

ARTICLE INFO

Article history:
Received 15 March 2011
Accepted 22 May 2011
Available online 23 June 2011

ABSTRACT

Accurate modeling of irradiation damage processes is important to predict materials performance in nuclear environments. The mean-field rate theory (RT) approach has been and remains the standard method for calculations of the kinetics of damage accumulation under irradiation. Despite its many advantages, when using RT, very large numbers of ordinary differential equations (ODEs) need to be solved if one is interested in the kinetics of complex defect populations containing defect clusters made up of constituent defect species of different types, *e.g.* He, H, O, alloying impurities, etc. Here we present a stochastic variant of RT, which we term stochastic cluster dynamics (SCD), intended as an alternative to the standard ODE-based implementation. SCD obviates the need to solve the exceedingly large sets of ODEs and relies instead on sparse stochastic sampling from the underlying kinetic Master Equation. The new method evolves an integer-valued defect population in a finite material volume. In this paper we describe the general ideas behind the SCD method, give essential details of our numerical implementation and present SCD simulations that verify the new method against standard RT implementations on two well characterized material models. We then apply the method to simulate triple beam irradiation experiments of heavy Fe ions, He, and H on model ferritic alloys up to a dose of 1 dpa.

1. Introduction

For the last four or so decades, researchers in nuclear materials have relied on the rate theory method (RT) for predictions of radiation damage accumulation in reactor materials. Also known as *master equation* or *cluster dynamics* method, RT is a mean-field approach in which the material microstructure is treated as a spatially-homogeneous effective medium with embedded effective sinks and sources for defect species [1–4]. Rate theory models are formulated as sets of ordinary differential equations (ODEs) describing the production and removal of point defects and defect clusters, and the corresponding evolution of the microstructure. Predictions are obtained by simultaneously integrating the ODE system for a given model.

The very definition of RT above points to its intrinsic limitations and strengths. Rate theory calculations are capable of providing predictions of high-dose irradiation on reactor timescales [5], but its computational efficiency is achieved at the expense of neglecting fluctuations and correlations in the evolving microstructure. More recent kinetic Monte Carlo (kMC) models can overcome this shortcoming of RT by considering the material microstructure in atomistic or nearly-atomistic detail [6–8]. By resolving every atomic jump, kMC models can reproduce finite-volume fluctuations and correlations in the evolving defect microstructure. However, the computational cost associated with kMC simulations makes them prohibitive to study reactor-relevant irradiation doses [9]. A useful compromise would then be to focus attention on improving the accuracy of rate theory models while, at the same time, retaining their computational efficiency.

In addition to ignoring finite-volume fluctuations and spatial correlations, the standard RT method suffers from a known but rarely discussed limitation related to cluster species complexity. In realistically complex materials, the kinetics of cluster populations are strongly affected by the interaction of irradiation defects and transmutation products with alloy elements and impurities. For example, vacancy diffusion in steels is known to depend on C content and other impurities [10]. Also, Cu clustering and precipitation in reactor pressure vessel steels is strongly influenced by Ni and Mn content, and their co-precipitation kinetics [11]. Another notable example is the bubble growth kinetics in materials co-implanted with two or more gaseous species, which is known to result in enhanced swelling [12,13]. Thus, in many technologically relevant situations it is important to consider complex clusters containing multiple component species (defects, gas atoms, solute atoms, etc.).

In the standard RT formulation, a faithful representation of the time evolution of such complex cluster populations entails writing and solving exceedingly large ODE systems, one equation for each combination of atomic species. Lumping clusters into prescribed

* Corresponding author.
E-mail address: marian1@llnl.gov (J. Marian).

0022-3115/$ - see front matter © 2011 Elsevier B.V. All rights reserved.
doi:10.1016/j.jnucmat.2011.05.045

size bins [15,16] has been shown to reduce the computational complexity of RT calculations in cluster-size space for two-dimensional species (vacancies plus He atoms) [14]. However, following the same coarse-graining strategy into still higher dimensions is limited by *combinatorial explosion*, *i.e.* the exponential growth of the size of the ODE system with the number of dimensions of the cluster-size space. Since the computational cost of RT calculations is defined by the total number of ODEs, handling multi -dimensional cluster populations will inevitably lead to coarser grids, thus under-resolving potentially important details of the cluster size distribution. Overcoming this dimensionality challenge requires truncating and approximating the tails of the evolving cluster-size distributions, which, in a multi-dimensional case, can become rather cumbersome and sometimes inaccurate [17]. Consequently, RT calculations have been limited so far to relatively simple material models in which defect populations have no more than two and, in most cases, just one size dimension.

The purpose of this paper is to demonstrate how the limitation of combinatorial explosion can be surmounted by recasting the rate theory method into a discrete stochastic framework that operates with integer-valued defect populations in a finite material volume, rather than with fractional defect concentrations in an effective medium. The advantage of using discrete populations is that the computational complexity of the simulations is no longer determined by the complexity of defect species (clusters), but rather by the selected simulation volume. This is the idea behind the *stochastic simulation algorithm* (SSA), originally developed by Gillespie for chemical reaction networks [18]. The SSA has since gained wide acceptance and become a dominant simulation method in biochemistry and cell biology [19], but its application to other fields has remained slow. This paper is an attempt to extend it to nuclear materials simulations. In what follows, we refer to our extension of the SSA as the *stochastic cluster dynamics* method (SCD).

2. The stochastic cluster dynamics method

The origins of standard RT and the SSA can be traced to the same fundamental reaction–diffusion master equation (ME). For RT, the mean-field assumption permits a drastic reduction of the ME leading to a set of non-linear ODEs for the individual components of the cluster populations. Along the way, in order to obtain the needed equations for cluster concentrations, all spatial correlations among defects clusters are ignored and finite-volume fluctuations are suppressed by taking the limit of infinite volume. The resulting ODEs for the average cluster concentrations are of the following form:

$$\frac{dC_\nu}{dt} = \Gamma_\nu - \sum_\mu R(\nu \to \mu) C_\nu + \sum_\mu R(\mu \to \nu) C_\mu - \sum_{\lambda\mu} K(\mu + \nu \to \lambda) C_\nu C_\mu + \sum_{\lambda\mu} K(\lambda + \mu \to \nu) C_\lambda C_\mu \quad (1)$$

where the first term on the r.h.s, Γ_ν, is the insertion rate (source term) of defect species ν. The second and third terms correspond to single species (1st order) reactions of conversion to and from species μ, respectively. The fourth and the fifth terms correspond to two species (2nd order) reactions leading to removal and creation of species ν, respectively. Following the notation in Ref. [4], species index ν is understood to be a shorthand notation for arbitrarily complex species $\nu = \{ijkl\ldots\}$ in which index $i = 0, \pm 1, \pm 2, \pm 3, \ldots$ is the number of self-interstitial atoms (SIA) (+) or vacancies (−) in cluster ν, and indices $j, k, l, \ldots = 0, 1, 2, 3, \ldots$ is the number of atoms of some other cluster elements, *e.g.* He, H, C, etc. Given that C_ν are concentrations, *i.e.* the average number of defect species ν per unit volume, the rate constants must be expressed in the following units: $m^{-3}\,s^{-1}$ for $\{\Gamma\}$, s^{-1} for $\{R\}$, and $m^3\,s^{-1}$ for $\{K\}$.

2.1. The stochastic simulation algorithm

The key difference between the standard RT and the SSA is that, rather than writing and solving the rate equations (ODE system) for average defect concentrations in an infinite medium, integer-valued populations N_ν of chemical species in a finite volume V are considered. Then, instead of integrating the ODE system forward in time, the SSA evolves the population stochastically, one reaction at a time. Over the years Gillespie has presented substantial theoretical justification for his method [20]. In particular, he showed that the SSA is equivalent to standard RT in the sense that:

$$\lim_{V\to\infty} \frac{N_\nu}{V} = C_\nu \quad (2)$$

At the same time, Gillespie convincingly argued that his method is more faithful to the underlying ME than standard RT. In particular, because the evolution given by the SSA is stochastic, it reproduces finite volume variations (fluctuations) in species population that are averaged out in the standard RT. According to Gillespie, the SSA is only accurate when the chemical components present in volume V are *well-stirred*, *i.e.* it is valid only for *reaction controlled* kinetics. This assumption is generally accurate for bimolecular reactions in gaseous mixtures of reactants. However, in condensed matter systems the overall bi-molecular reaction rate is often *diffusion controlled*, *i.e.* limited by slow diffusion of species that react instantly upon collision. Thus, the applicability of the SSA in its original form to reactive systems where diffusion plays an important role is not guaranteed. At the same time, as we show in Section 2.2, it is possible to recast the RT formulation into a form of stochastic algorithm that reproduces the solution of standard rate theory in the limit $V \to \infty$. Therefore, the accuracy (or lack thereof) of the resulting stochastic method derives from that of standard RT, which, in turn, largely rests on the validity of the mean-field approximation for diffusion-controlled reactive systems representing irradiated materials.

Even though the mean-field assumption is usually thought to be valid for diffusion problems in $d > 2$, its validity in general diffusion–reaction systems in $d = 3$ is a subtle issue [21] and is only glossed over in the radiation damage literature. However, the purpose of this work is not to discuss the suitability of the mean-field assumption but, rather, to show how one can practically recast a standard RT model into a SSA-type stochastic algorithm. The key step in our reformulation is to convert the reaction rates appearing in the standard RT into rates usable in a stochastic setting. To illustrate this rate conversion, it is sufficient to multiply both sides of Eq. (1) by V and express the concentrations as integer numbers of species according to Eq. (2), *i.e.* $N_\nu = V{\cdot}C_\nu$. The resulting converted rate equations are then:

$$\frac{dN_\nu}{dt} = V\Gamma_\nu - \sum_\mu R(\nu \to \mu) N_\nu + \sum_\mu R(\mu \to \nu) N_\mu - \sum_{\lambda\mu} \frac{K(\mu + \nu \to \lambda)}{V} N_\nu N_\mu + \sum_{\lambda\mu} \frac{K(\lambda + \mu \to \nu)}{V} N_\lambda N_\mu \quad (3)$$

If we redefine the rates as: $\widetilde{\Gamma} = V\Gamma$, $\widetilde{R} = R$, and $\widetilde{K} = K/V$, then

$$\frac{d}{dt} N_\nu = \widetilde{\Gamma}_\nu - \sum_\mu \widetilde{R}(\nu \to \mu) N_\nu + \sum_\mu \widetilde{R}(\mu \to \nu) N_\mu - \sum_{\lambda\mu} \widetilde{K}(\mu + \nu \to \lambda) N N_\mu + \sum_{\lambda\mu} \widetilde{K}(\lambda + \mu \to \nu) N_\lambda N_\mu \quad (4)$$

These equations are only symbolic and do not imply forward time integration. Rather, one can regard Eq. (4) as the physical

representation of a catalog of possible events characterized by $\{\widetilde{\Gamma}, \widetilde{R}, \widetilde{K}\}$ that can be sampled using any exact kMC algorithm, such as BKL [22]. In fact, Gillespie independently proposed an algorithm essentially identical to BKL that correctly samples stochastic trajectories from the distributions implied by Eq. (4) [18]. Other kMC algorithms developed for exact sampling of ME may also be used [23]. Here we emphasize again that, regardless of the kMC algorithm chosen, the species population is evolved stochastically, one reaction at a time.

As should become evident from the subsequent discussion, the single most important potential advantage of the SSA is that, at any given point in the simulation, only defect populations with $N_v \neq 0$, *i.e.* those that actually exist in the finite volume V, are kept track of. By contrast, in standard RT, all possible species whose evolution is included in the ODE system must be dealt with at all stages of the ODE integration. Thus, the principal advantage of the SSA method is that the number of existing species is controlled by the simulation volume V rather than by the combinatorial complexity of the RT model. This situation is just another manifestation of the power of the Monte Carlo method that was originally proposed for efficient numerical calculations of multi-dimensional integrals: rather than covering the whole multi-dimensional space with a grid, the Monte Carlo method obtains a converging estimate of the integral by sparse sampling of the integrand values in randomly selected points [23].

2.2. Recasting the rate theory of damage accumulation in stochastic terms

2.2.1. 0th-order reactions

In the context of irradiation damage, the 0th-order reactions are used to represent the source of initial defects or implanted species. Generally, the rate of insertion of a given defect subspecies is expressed in displacements per atom per second (dpa s^{-1}), whereas ion insertion (*e.g.* He, H, etc.) is simply given in terms of ions per second. These processes are all considered as stochastic Poisson events with their corresponding rates. A full description of how damage is inserted in SCD simulations is given in Section 4.1.

2.2.2. 1st-order reactions

1st-order reactions represent events of cluster dissociation and defect absorption at sinks. Cluster dissociation is usually taken to proceed according to classical nucleation theory, *i.e.* via a quasi-equilibrium exchange of monomers with the remote (mean-field) monomer atmosphere [24]. It is also possible to obtain the rate of monomer emission from considerations not involving quasi-equilibrium, as shown below. The monomer emission rates used in the mean-field RT calculations are effective, meaning that the rate value entering the mean-field equations must be adjusted to reflect that some monomers that split off an emitting cluster, will return to the same cluster even if there is no cluster-monomer attraction. This correlation effect is purely geometrical: a point-like random walker placed at a standoff distance d away from the surface of spherical cluster, will return to the same cluster with probability $\frac{r}{d+r}$ [25]. Thus, even though the rate of monomer emission events should be approximately proportional to the cluster surface $4\pi r^2$, the effective rate at which the cluster supplies monomers to the remote atmosphere should be corrected by the fraction of non-returning monomers $\frac{d}{d+r}$. The effective rate of monomer emission is thus written as:

$$R_n = \frac{d}{d+r}\frac{4\pi r^2}{\alpha a_0^2} \nu_0 \exp\left(-\frac{E_b(n)+E_m}{k_B T}\right) \tag{5}$$

where d is typically the first nearest-neighbor jump distance, and the term $\frac{4\pi r^2}{\alpha a^2}$ is an approximate count of all distinct locations on the cluster surface from which a monomer may be emitted. Here, α is a dimensionless geometric parameter of the order of unity, and a_0 is the lattice parameter. ν_0 is the attempt frequency, $E_b(n)$ is the binding energy of a monomer to a cluster of size n, E_m is the monomer migration barrier, k_B is Boltzmann's constant and T is the temperature. Obviously, the effective monomer emission rate scales as $\sim r$ for large clusters ($r \gg d$), as is the case when quasi-equilibrium is assumed.

Defect absorption by dislocations, grain boundaries, precipitate particles and other elements of the material microstructure, is traditionally included into sink terms of the following form:

$$R = S D_v C_v,$$

where S is the so-called sink strength parameter reflecting the efficiency of a given sink in removing mobile species v, and D_v and C_v are the diffusion coefficient and the concentration of the same mobile species. The rate appropriate for our discrete-valued implementation is simply:

$$R = S D_v N_v.$$

In this work we have considered dislocation and grain boundary sinks, whose contribution to S is, respectively, $S = S_d + S_g = \rho + 6\sqrt{\rho}/L$, where ρ is the dislocation density and L is the grain size. Appropriate bias factors for interstitial and vacancy-type defects can multiply S_d and S_g.

Alternatively, the same sinks can be included in the model more explicitly, *i.e.* in the form of 2nd-order reactions, as detailed in Section 2.2.3 below. Which of the two alternative forms to use —1st or 2nd-order— to describe sinks can have an effect on model accuracy and computational efficiency.

2.2.3. 2nd-order reactions

The 2nd-order reaction term in RT accounts for the various mechanisms involving collisions of two defect cluster species, *e.g.* SIA-vacancy annihilation, SIA absorption by an interstitial cluster, vacancy aggregation, etc. Terms describing such binary reactions are often taken directly from Smoluchowski's stationary solution for the collision rate between two spherical particles [26]:

$$4\pi(r_\mu + r_\nu)(D_\mu + D_\nu) C_\mu C_\nu,$$

where r_μ and r_ν are the reaction radii of the reacting species, D_μ and D_ν are the corresponding diffusion coefficients, and C_μ and C_ν are the respective particle concentrations. The terms appropriate for our discrete valued model are then simply:

$$\frac{4\pi(r_\mu + r_\nu)(D_\mu + D_\nu)}{V} N_\mu N_\nu.$$

For more accurate description of binary association mechanisms in irradiated materials, the 2nd-order terms sometimes include corrections to account for possibly different (non-spherical) shapes of interacting clusters, their mutual attraction or repulsion, and for one-dimensional diffusion of some clusters [27,28], *e.g.* SIA clusters in metals.

In our discrete model the binary terms are written as:

$$\begin{array}{l} \frac{4\pi r_{\mu\nu}}{V} f_{\mu\nu} N_\mu N_\nu, \text{ if } \nu \neq \mu \\ \frac{4\pi r_{\mu\nu}}{V} f_{\mu\nu} \frac{N_\nu(N_\nu-1)}{2}, \text{ if } \nu = \mu \end{array} \tag{6}$$

where $r_{\mu\nu}$ is an interaction radius that reflects the shapes of one or both collision species as well as their possible attraction or repulsion, and the factor $f_{\mu\nu}$ takes a different form depending on the dimensionality of motion of the species involved. One can consider three distinct cases relevant for simulations of radiation damage accumulation:

(i) Both species μ and ν diffuse isotropically in 3D.
(ii) One species μ diffuses one-dimensionally and species ν diffuses isotropically in 3D.

(iii) Both species diffuse in 1D along two non-parallel directions.

In what follows we limit consideration to case (i) so that $f_{\mu\nu} = (D_\mu + D_\nu)$ and $r_{\mu\nu} = r_\mu + r_\nu$.

As discussed above, it is possible to treat defect absorption at sinks as second order reactions. As an example, consider (mobile or immobile) species μ such that its number count N_μ is not affected by collisions with defect species ν. Such a second order reaction term can be written as $\frac{4\pi r_{\mu\nu} f_{\mu\nu} N_\mu D_\nu}{V} \cdot D_\nu N_\nu$ and its effect on the kinetics of species ν will be precisely the same as that of a first order sink term with ideal (constant) sink strength $S = \frac{4\pi r_{\mu\nu} N_\mu}{V}$. Because the number count of species μ remains unchanged, it is more efficient to treat such reactions as first order. Even when N_μ does change in collisions with species ν, their reaction can be approximately treated as first order for computational efficiency, for as long as variations in N_μ remain small compared to the species number count itself, $\delta N_\mu / N_\mu \ll 1$. Species μ should be updated if and when the accumulated change δN_μ reaches a certain fraction of N_μ (in the context of the SSA, approximations of this kind are referred to as *tau-leaping* [29]). Conversely, some of the elements of material microstructure traditionally treated as ideal sinks, *e.g.* dislocations, may be more accurately described as non-ideal sinks whose properties (and strength) are changing as a result of reactions with other defect species. Such a sink requires that its strength parameter S be occasionally updated (as in tau-leaping) or may even deserve to be promoted into a second order binary reaction.

2.3. Implementation

In adapting the SSA to irradiation damage simulations, efficient handling of evolving populations data is crucial. The numbers and types of defect species present at the beginning of an SCD simulation, *e.g.* in a fresh material, often change dramatically into the late stages of damage accumulation. An overwhelming majority of defect inserted by the damage source annihilate with each other or are absorbed at sinks, and only a small fraction of defects survive to form clusters giving rise to damage accumulation. Owing to a typically large disparity in defect mobilities and to specific properties of the damage source, in some instances some defect species can be present in very large numbers whereas other defect species are represented only sparsely. Furthermore, the relative weights of various species sub-populations can change dramatically as the simulation proceeds. Thus, efficiency of SCD simulations requires both efficient storage of and fast searches through populations data tables, parts of which are dense while others are sparse. Among numerous data structures available, we chose to use hash tables for their combination of compact storage, fast searches and flexibility.

Hash tables support $\mathcal{O}(1)$ operations of types *add*, *find*, and *delete* on key-indexed data structures. In our current code we employ the UTHASH macros developed by Hansen for C programs [30]. Two hash tables are co-managed in each compute cycle: the first one is the main hash table that contains all species (mobile and immobile) in the system at any given time and the second hash table contains only the mobile species. The entire reaction matrix of the 2nd-order reaction rates is constructed (or updated) once per cycle, with the columns built by referencing the first hash table for all reactive species and the rows built by referencing the second hash table for the mobile species. A flow diagram of our SCD code is given in Fig. 1.

Even though, as in standard RT, SCD lacks any notion of spatial positions, one has to be careful in choosing an appropriate value for the simulation volume. For example, in order to prevent build-up of spurious self-correlations one may wish to always maintain the radius of the simulation volume $V^{\frac{1}{3}}$ larger than the length of the diffusion path of any mobile defect. In the beginning of a simulation, especially in the absence of sinks, the defects are sparse and their diffusion length can be large. Subsequent insertion of irradiation sub-cascades produces increasingly more defects making their collisions more frequent and thus reducing the diffusion lengths. Perhaps most relevant are cases when sinks are present from the beginning. In those instances, the box size should be selected so that the combined strength of all sinks S_ν^{tot} for each mobile species ν is sufficiently large to make the mean diffusion lengths $\lambda_\nu \sim S_{\nu,tot}^{-\frac{1}{2}}$ smaller than the simulation box size, *i.e.* $\lambda_\nu < V^{\frac{1}{3}}$ for every mobile species. Since over the course of a SCD simulation defect clusters tend to accumulate, the cost of each subsequent Monte Carlo cycle rises owing to increasingly more numerous reaction rate updates. At the same time, the diffusion lengths λ_ν tend to decrease for mobile species which may allow a reduction in V to manage the simulation cost. Such volume reduction can be achieved by rescaling all the species populations by a factor V_2/V_1, where V_1 and V_2 are the original and rescaled volumes, respectively, and randomly initializing the resulting populations within allowable statistical fluctuations.

3. Cross verification with standard rate theory

In this section we carry out SCD simulations to verify the method by comparison to traditional RT calculations performed on the same models. Before presenting the results it is useful to recall in what sense SCD and RT simulations can be deemed equivalent. A RT calculation is a numerical solution of an ODE set for volume-averaged concentrations of defect and cluster species. As such, errors in the RT simulations are owed to numerical integration. Such errors are often assumed to be negligible, in which case the resulting numerical solution is considered to be indiscernible from a hypothetical exact solution of the same ODE set. In contrast, there is no truncation errors or any other numerical errors in counting the integer-valued populations of defect species in SCD. Instead, the error bars of any function in a SCD simulation are computed as the standard deviation of the same function over a series of stochastic simulations, each of which is performed in the same simulation volume V using a different sequence of random numbers. A SCD simulation is then nothing but a single realization of the stochastic process represented by the master equation. Except in the hypothetical (and impractical) case of a SCD simulation in an infinite simulation volume, standard deviations should not vanish even in the asymptotic limit of very large number of independent SCD simulations. Instead, the standard deviations computed over a series of SCD simulations reflect finite-volume variations in the evolving species subpopulations and, as such, contain useful information that the RT solution lacks. Thus, the best one can do in terms of cross-verification of RT and SCD simulations is to ensure that the numerical solution of the former is within the standard deviation of the latter.

First we consider a simple model of damage accumulation in α-Fe subjected to electron irradiation, as detailed in Ref. [31]. The model is of a 364-nm thick film of material with no pre-existing impurities or defects other than the two film surfaces that serve as the only sinks in the model. Barbu et al. [31] used this simple model to compare RT calculations with two different methods for space-resolved kMC simulations. Taking advantage of its low computational complexity, here we use the same simple model for cross-verification of RT calculations and SCD simulations. We refer to the original paper for a full description of the model and its numerical parameters. Fig. 2 shows the damage accumulated after 120 s of irradiation at a nominal rate of 1.5×10^{-4} dpa s^{-1}, at six different temperatures for V and SIA clusters. Our primary interest here is to compare the RT points reported in the paper (labeled 'CD', for *cluster dynamics*, by Barbu et al.) with our SCD predictions. SCD

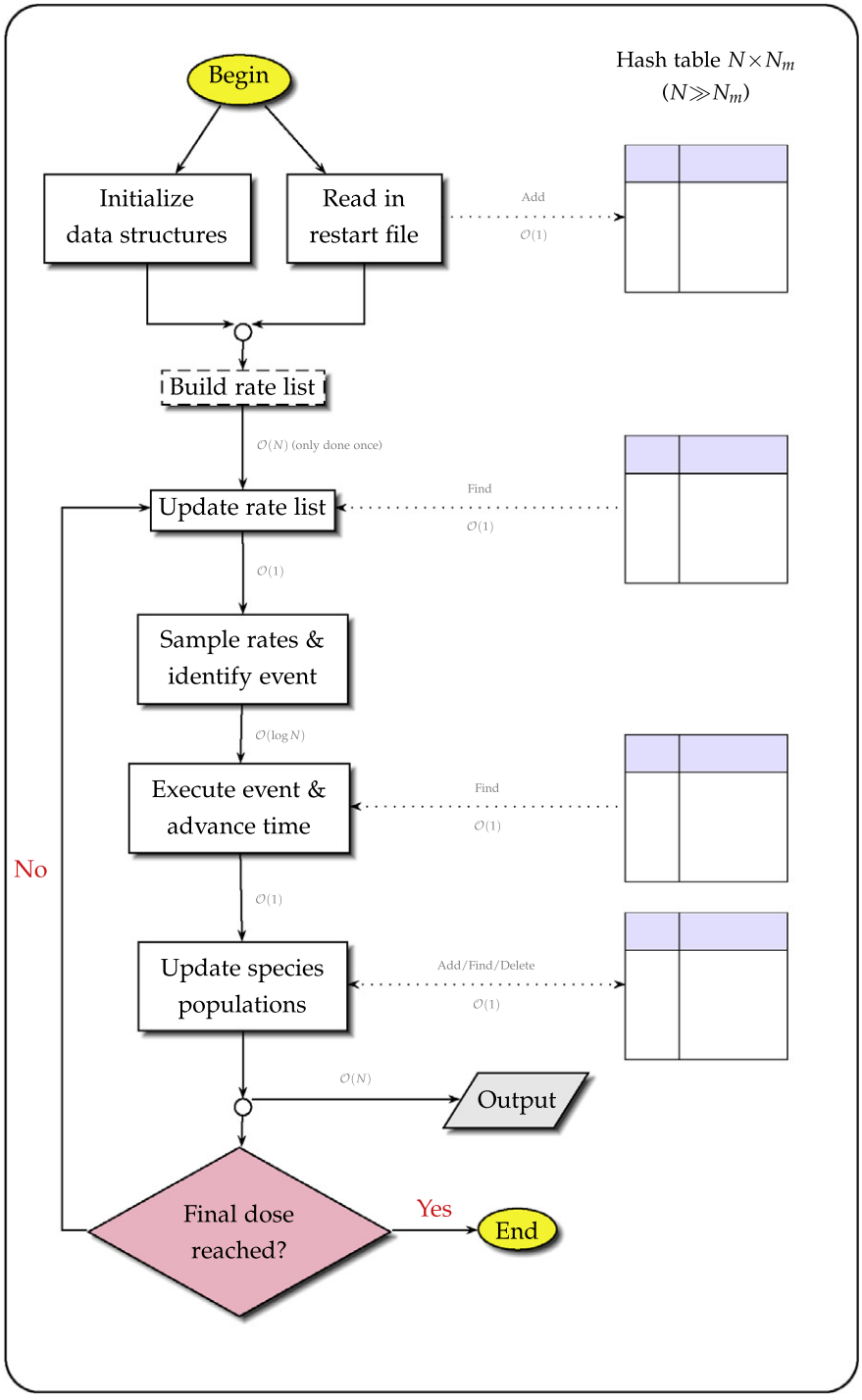

Fig. 1. Flow diagram of the SCD code used in the simulations discussed in Section 4. N and N_m are the total and mobile numbers of species. The computational cost associated with each operation is shown for reference.

results for both the SIA cluster (Fig. 2a) and vacancy cluster populations (Fig. 2b) are seen to coincide with the rate theory results within the standard deviations obtained by averaging over 20 independent SCD simulations at each temperature. [1] The apparent discrepancy between the RT and the SCD results in regards the vacancy cluster concentrations at lower temperatures (open circles in Fig. 2b) is not clear, although it could stem from using different capture radii for cluster absorption of vacancies.

Next we turn to another model of α-Fe subjected to similar conditions of electron irradiation [9]. This second model pertains to a bulk polycrystal containing dislocations, *i.e.* both grain boundaries and dislocations serve as sinks of mobile defects with sink strength parameters assigned according to the standard theory [33,34]. This time, the SCD simulation volume was chosen so as to resolve the lowest defect concentrations reported by Stoller et al. [9]. In this case this concentration was $5.8 \times 10^{18}\,\mathrm{m}^{-3}$, corresponding to

[1] At some temperatures, the mean defect densities obtained by averaging over the series of SCD simulations (solid circles) are visibly shifted towards the upper bounds of wide uncertainty intervals. This is primarily due to low defect counts obtained in some simulations at the corresponding temperatures, which pushes the lower bounds of the error bars to rather small values when plotted in logarithmic scale [32].

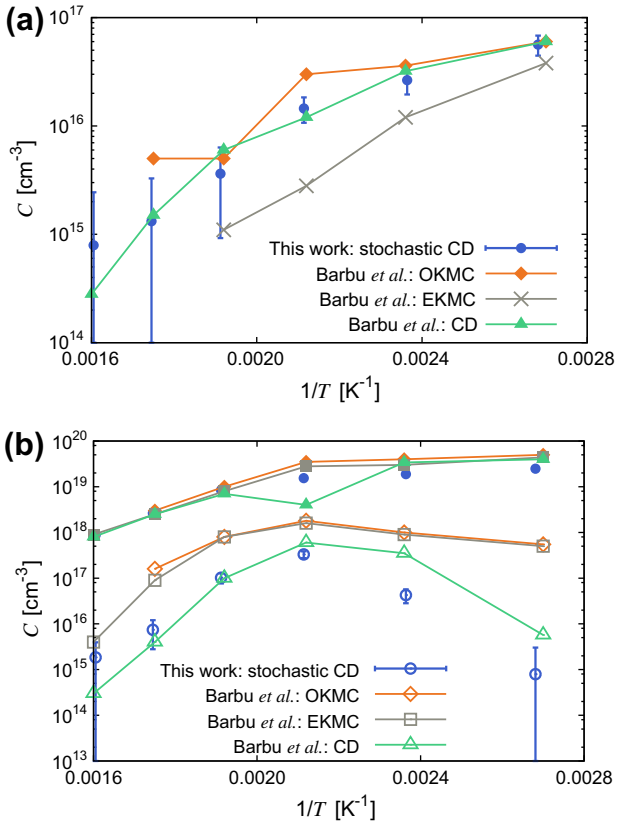

Fig. 2. Arrhenius plot of the number density of defects after 120 s of irradiation for the model proposed by Barbu et al. [31]. Solid symbols correspond to total defect concentrations, while open ones refer only to clusters with $n > 1$, *i.e.* not including monomers.(a) SIA cluster concentration as a function of temperature. The error bars represent the standard deviation of the mean value (solid circles) and are obtained from 20 independent SCD calculations. (b) Vacancy cluster (open circles) and total vacancy (solid circles - including monovacancies) concentrations as a function of temperature. The error bars represent the standard deviation of the mean values in each case and are obtained from 20 independent SCD calculations.

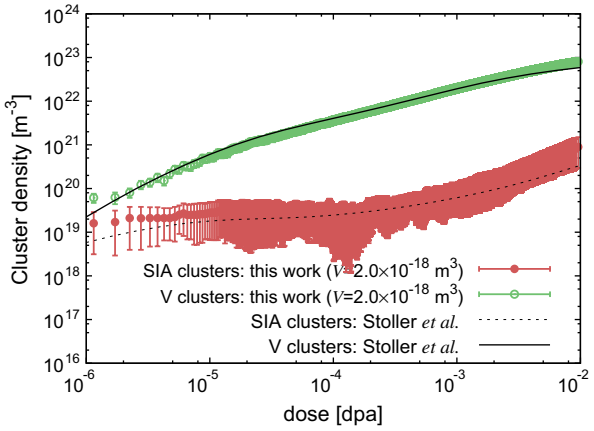

Fig. 3. Dose dependence of vacancy and interstitial cluster densities for case 3 in Ref. [9]: comparison between the standard RT and SCD simulations performed in a fixed volume of 2.0×10^{-18} m^{-3}. Each SCD data point and its statistical variance are obtained by averaging over five independent stochastic simulations starting from the same initial condition of zero defect counts. The open circles are the average vacancy cluster densities, while solid circles are the average SIA cluster densities from the SCD simulations. The corresponding solid and dashed lines are the RT solutions as given by Stoller et al. [9].

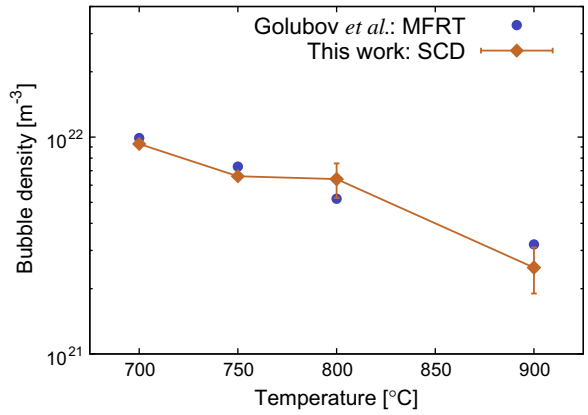

Fig. 4. The number densities of He bubbles nucleated in the model of austenitic steel proposed in [14] after 360 s of annealing at four different temperatures following pre-implantation with He ions to 40 appm at room temperature. Solid circles are the RT calculation results, while diamonds are the bubble densities obtained by averaging over 8–15 independent SCD simulations in a volume of 2.5×10^{-20} m^{-3}.

$V = 2.0 \times 10^{-18}$ m^{-3}. Increasing the simulation volume simply decreases the magnitude of the statistical uncertainties in the defect concentrations, at an additional computational cost. As is clear from the plots shown in Fig. 3, the RT solution agrees with the SCD results within the statistical variance of the latter.

The comparisons presented in Figs. 2 and 3 provide verification of our SCD approach for two relatively simple models where defect populations can be described by a single size index. As noted earlier, defect population models with more than one size index present challenges for RT calculations due to the large number of ODEs required to represent the evolving population of complex defect species. To date, very few RT simulations for models with two size dimensions have been reported [14,35], and none for three or more. Fig. 4 compares SCD and RT calculations for a two-dimensional model proposed by Golubov et al. [14] for the kinetics of gas bubble nucleation and growth in austenitic steels implanted with 40 appm of He at room temperature. Each of the four data points in the figure represents the number density of He bubbles nucleated after 360 s of annealing at elevated temperature following pre-implantation. As before, all material parameters in the SCD simulations are set to precisely the same values as in the original model, while the simulation volume $V = 2.5 \times 10^{-20}$ m^{-3} and the number of independent SCD simulations (between 8 and 20) are chosen so as to resolve the minimum defect concentration observed in the RT cases within reasonable statistical variance.

4. Multispecies SCD simulations

The main objective of this section is to demonstrate how the SCD method can be used for numerical simulations of damage evolution in complex materials containing defect species with multiple size attributes. Recent triple-beam irradiation experiments in which heavy ions were co-implanted with He and H ions in an attempt to reproduce He and H-to-dpa ratios created by fusion neutrons present a relevant testbed for our approach [36,37,13]. A common observation in all these studies was that co-implantation of displacement damage, He and H enhances swelling with respect to cases where only heavy ions and one gaseous species are implanted. This synergism, by which co-implanted He and H with damage conspire to enhance swelling, poses an as-of-yet unresolved puzzle for which SCD calculations can provide useful insights. Inspired by the experiments of Tanaka et al. [13], here we perform calculations of damage accumulation in FeCr alloys co-implanted with 10.5-MeV Fe ions and 10 and 40 appm/dpa of He and

Table 1
Material and simulation parameters used for the triple ion-beam irradiation simulations.

Material parameters:	Symbol		Units
Atomic density	ρ_a	8.5×10^{28}	[m^{-3}]
Lattice parameter	a	2.9×10^{-10}	[m]
Dislocation density	ρ_d	1.5×10^{15}	[m^{-2}]
Grain size	S_g	10^{-6}	[m]
Irradiation parameters:			
Temperature	T	27 and 510	[°C]
dpa rate		1.6×10^{-3}	[s^{-1}]
Fe ion energy	E_i	10.5	[MeV]
He/dpa ratio		10	[appm]
H/dpa ratio		40	[appm]
Simulation parameters:			
Volume	V	10^{-19}	[m^3]
SIA dislocation capture efficiency	Z_{di}	1.2	
Vacancy dislocation capture efficiency	Z_{dv}	1.0	
SIA grain boundary capture efficiency	Z_{gi}	1.0	
Vacancy grain boundary capture efficiency	Z_{gv}	1.0	

H respectively. Table 1 lists the parameters characterizing the irradiation conditions and the material microstructure as given by Tanaka et al.

4.1. Damage source term

Due to its stochastic nature, SCD can also treat collision cascades inflicted by ions and gas implantation as stochastic processes. In our current implementation, ion implantation and cascade damage are modeled as sequences of discrete Poisson events with the ion insertion rates adjusted to the nominal damage dose rate in dpa s^{-1} and to the gas implantation rate in appm/dpa. The primary displacement damage is generated from a Fe-recoil distribution obtained using the SRIM software package [38] for approximately 1000 Fe ions with the same incident energy of 10.5 MeV. According to the calculations, only about 14% or 1.45 MeV of the total incident energy is expended on lattice damage, with the rest lost in ionization via electronic stopping. The available 1.45 MeV are partitioned according to the cumulative probability distribution function (*cpdf*) shown in Fig. 5, which results in an average recoil energy of 2.14 keV.

Once an ion insertion event is selected in the main computation cycle (cf. Fig. 1), this *cpdf* is used to randomly sample the energies

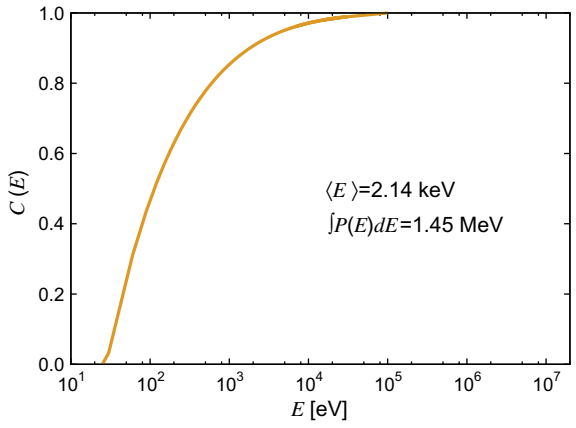

Fig. 5. Cumulative Fe recoil distribution as obtained from SRIM for 10.5-MeV Fe-ion irradiation assuming a threshold displacement energy of 25 eV. The average recoil energy and the total ion energy expended on creating damage (14% of total) are also shown. $C(E)$ is used to obtain random samples of the primary knock-on atom (PKA) energies E by solving $E = C^{-1}(\xi)$, where ξ is a random number uniformly distributed in [0,1). Note that $C(E) = \int_0^E \|P(E)\| dE$, where $P(E)$ is the recoil energy spectrum.

Table 2
Diffusion coefficients of the mobile species considered for the triple ion-beam irradiation simulations.

Species	D_0 ($m^2 s^{-1}$)	E_m (eV)	Reference
I_1	1.3×10^{-8}	0.25	[41]
I_2	351.6×10^{-8}	0.36	[41]
I_3	12.1×10^{-8}	0.14	[41]
I_4	12.3×10^{-8}	0.15	[41]
$n > 4$	$9.0 \times 10^{-7} n^{-0.6}$	$0.06 + 0.07 n^{-1.3}$	[42]
V_1	7.9×10^{-7}	0.60	[43]
V_2	3.5×10^{-8}	0.66	[44]
V_2–He_1	4.1×10^{-8}	0.27	[45]
V_1–He_2	3.3×10^{-7}	0.31	[46]
V_1–He_3	3.2×10^{-8}	0.30	[46]
V_1–He_4	2.1×10^{-9}	0.31	[46]
V_2–He_3	9.9×10^{-9}	0.53	[46]
He_1	2.8×10^{-8}	0.06	[46]
He_2	3.0×10^{-8}	0.08	[46]
He_3	1.0×10^{-8}	0.07	[46]
He_4	0.1×10^{-8}	0.05	[46]
He_5	1.6×10^{-9}	0.20	[47]
He_6	3.9×10^{-9}	0.28	[47]
H_1	1.5×10^{-7}	0.09	[48]

of multiple recoils, one PKA energy at a time, until the sum of all sampled recoil energies reaches 1.45 MeV. For each individual PKA, further randomization is performed to account for statistical variations in the number of defects and defect clusters generated in a collision cascade with a given recoil energy. Defect species are generated randomly *on demand* by sampling from discrete distributions parameterized to reproduce sub-cascade statistics collected by Malerba et al. [39,40]. In this fashion, the inserted defect populations originate from a rich statistical database constructed from hundreds of MD cascade simulations covering a wide range of recoil energies and temperatures.

4.2. Model parameters

Table 1 lists the parameters describing the host material, irradiation conditions and sink efficiencies used in simulations discussed in this section. The diffusivities and binding energies of various defects and clusters considered here are listed in Tables 2 and 3, respectively. In both tables, literature sources for each parameter type are listed in the rightmost column. Diffusion coefficients of all mobile defects and clusters are computed using an Arrhenius function: $D(T) = D_0 \exp\left(-\frac{E_m}{k_B T}\right)$, whereas the rates for monomer emission were computed using Eq. (5). The simulation volume in all cases was $V = 10^{-19}$ m^3.

For consistency with the microstructures used by Tanaka et al. [13], here we consider only two types of sinks: grain boundaries and dislocations. Due to the relatively small grain size and high dislocation density, the combined strength of all sinks in our model material is quite high. For dislocations, we assume a bias factor of 20% favoring the absorption of SIAs over that of vacancies, whereas the grain boundaries are assumed to be neutral sinks.

Next we describe the most salient features regarding the defect physics and microstructure considered in the SCD simulations. To parameterize our model we use, whenever possible, insights gained from recent atomistic simulations. Regarding defect mobilities, only mono and di-vacancies are assumed to be mobile. Once V_n–He_m clusters are formed, only certain combinations of n and m correspond to mobile species, as shown in Table 2. All clusters with more than two vacancies are considered immobile regardless of their He content, which is consistent with recent MD simulations of di-vacancy and V–He cluster diffusivity [44,46]. Due to the lack of any data on the mobility of V_n–H_m clusters, such defect

Table 3
Binding energies for all species used for the triple ion-beam irradiation simulations. E_{fi} = 3.8 eV and E_{fv} = 1.7 eV are the SIA and vacancy formation energies.

Species	E_b (eV)	Reference
I_2	0.80	[49]
I_3	0.92	[49]
I_4	1.64	[49]
$n > 4$	$E_{fi} - 5.06(n^{2/3} - (n-1)^{2/3})$	[50]
V_2	0.30	[49]
V_3	0.37	[49]
V_4	0.62	[49]
$n > 4$	$E_{fv} - 3.01(n^{2/3} - (n-1)^{2/3})$	[50]
V_1–He_1	2.4	[46]
V_n–He_m	$E_b(\mathrm{V}) = 1.59 + 3.01\log(\frac{m}{n}) + 2.70\log^2(\frac{m}{n})$	[46]
	$E_b(\mathrm{He}) = 2.20 - 1.55\log(\frac{m}{n}) - 0.53\log^2(\frac{m}{n})$	[46]
V_1–H_1	0.57	[51]
V_1–H_2	$E_b(\mathrm{V}) = 5.51$	[52]
	$E_b(\mathrm{H}) = 0.47$	[52]
V_2–H_1	$E_b(\mathrm{V}) = 4.54$	[52]
	$E_b(\mathrm{H}) = 0.57$	[52]
V_2–H_2	$E_b(\mathrm{V}) = 0.27$	[52]
	$E_b(\mathrm{H}) = 2.06$	[52]
V_2–H_2–H_1	$E_b(\mathrm{V}) = 1.98$	[53]
	$E_b(\mathrm{He}) = 3.38$	[53]
	$E_b(\mathrm{H}) = 1.35$	[53]

complexes are considered immobile for all non-zero values of n and m. For their part, SIA clusters of all sizes are assumed to be mobile with diffusivities given in Table 2. At the same time, all I_n–He_m clusters with $n, m > 0$ are assumed to have zero diffusivity irrespective of how He enters the complex (in substitutional or interstitial form), as suggested by two MD studies in which SIA clusters and He atoms were observed to react and form stable sessile complexes [54,55]. Although there is no direct evidence in the literature of reactions between SIA clusters and H atoms, the latter defect species are also assumed to form stable SIA–H complexes with zero mobility. At this stage of method development, we choose to disregard one-dimensional diffusion of SIA clusters and assume, for simplicity, that all mobile defect species move three-dimensionally.

With respect to cluster dissociation reactions, we have assumed that all I_n–He and I_n–H clusters are thermally stable following Ventelon et al., who have reported binding energies from 1.3 to 4.4 eV for small SIA–He clusters [54]. As we shall see, this assumed stability of SIA–He/H complexes is essential for the observed accumulation of SIA dislocation loops in our model material with the increasing irradiation dose. For V_n–H_m clusters, for lack of a better approximation[2], we have assumed that H atoms cannot escape from their host vacancy clusters. However, this is not inconsistent with the expectation that atomic H readily reacts to form molecular H_2 that is then retained in the bubbles [56] The numerical parameters pertaining to the mechanisms described above are given in Tables 1–3.

In the next two sections we present SCD results for four irradiation conditions: two involving implantation at room temperature (300 K) and two at 783 K (which is the temperature at which Tanaka et al. observed maximum swelling). At each temperature two irradiation scenarios are considered: in one case all gas atoms (He and H) are implanted in the form of interstitials while in the other case all are implanted as substitutional impurities. Thus, our simulations explore the extremes of the range in which the form of the gas implantation source (interstitial or substitutional) can affect the resulting kinetics of damage accumulation. As shall be reported in a forthcoming publication, a more realistic source

[2] To our knowledge, there are no reported binding energetics for V_n–H_m clusters in α-Fe in the literature.

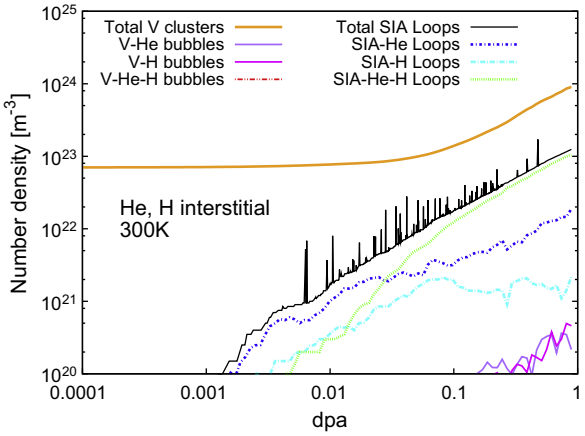

Fig. 6. Accumulation of defect species as a function of dose at 300 K for the case when He and H are implanted as interstitial atoms.

term for He implantation should contain a fraction of gas in the substitutional form with the balance of He in the interstitials [57]. All calculations described below were carried out to a total dose of 1 dpa.

4.3. Simulation of damage accumulation at 300 K

Fig. 6 shows the simulated kinetics of damage accumulation for the case where all He and H are inserted as interstitial impurities. The figure reveals different incubation doses for SIA clusters and bubbles. Small vacancy clusters, mostly in the form of V_2 and V_3, appear as soon as irradiation is commenced. Due to their reduced mobility, these small vacancy clusters reach a state of quasi-equilibrium whereby their dissociation and annihilation with SIAs is balanced against their generation in displacement cascades. This behavior persists up to a dose of 0.01 dpa, at which point the total vacancy concentration grows steadily again. The causes for this behavior are found in the co-evolution of the vacancy population with other defect species, and are explained in the following.

In the beginning, all He and H atoms migrate to and are absorbed at sinks (dislocations and grain boundaries) without finding any other defect species with which to react. However, at a dose of approximately 0.002 dpa, collisions between He atoms and vacancy clusters start occurring, resulting in the formation of substitutional V–He clusters. This is followed by the corresponding formation of substitutional V–H at approximately 0.005 dpa. Following these reactions, fast-diffusing SIA clusters begin to find immobile substitutional He and H, and accumulation of SIA–He and SIA–H clusters commences in earnest. These clusters are immobile, which allows them to continue to experience further reactions with mobile interstitial He and H, and with other small, cascade-generated SIA clusters. In this fashion, the size and number density of these defects grow very rapidly and, eventually, all become populated with He and H atoms. Such mutually-trapped SIA–He–H loops continue to grow,[3] thus effectively increasing the total sink strength (here we regard the growing SIA loops as neutral sinks). This steadily growing sink strength shifts the condition of quasi-steady state [58] to progressively higher vacancy/interstitial ratios where vacancy clusters begin to accumulate again up to densities of the order of 3.0×10^{24} m^{-3} at 1 dpa. Notably, some of the substitutional He and H atoms serve as seeds for gas bubble nucleation through accumulation of more vacancies and gas atoms. The

[3] The SIA clusters are assumed to be disc-shaped dislocation loops and, hence, their radii grow relatively rapidly with increasing SIA count: $r_n = \sqrt{\frac{\Omega_a n}{\pi b}}$, where Ω_a is the atomic volume and b the Burgers vector, cf. Fig. 8.

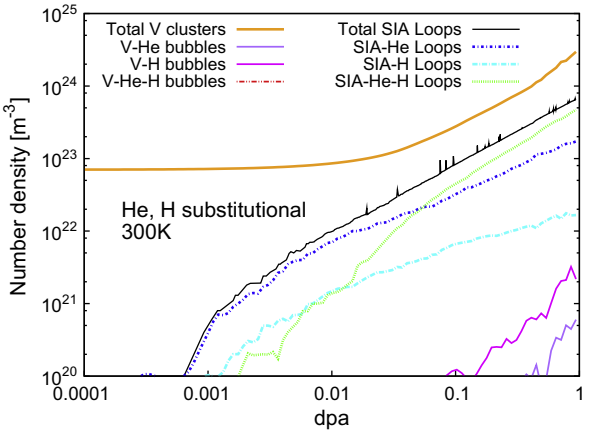

Fig. 7. Accumulation of defect species as a function of dose at 300 K for the case when He and H are implanted as substitutional atoms.

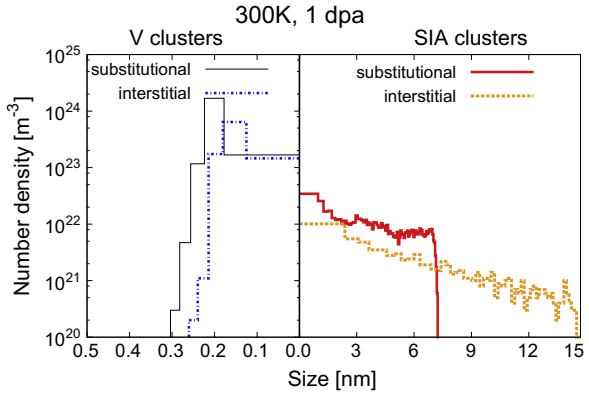

Fig. 8. Defect cluster size distributions developed under triple-beam irradiation to a dose of 1 dpa for the cases where He and H are implanted either as interstitials (dotted lines) or substitutionals (solid lines). V clusters include bubbles (vacancies plus He or H or both) as well as gas-free vacancy clusters.

incubation dose for bubble nucleation is approximately 0.15 dpa for V–He clusters, and 0.3 dpa for V–H clusters. No mixed V–He–H clusters were observed within the timescale of the SCD simulation, but it is perhaps reasonable to assume that the incubation dose for such mixed-gas clusters is larger than 1 dpa. Fig. 8 shows the size distributions for V and SIA clusters reached at the end dose of 1 dpa.

Fig. 7 shows the simulated kinetics of damage accumulation for the hypothetical case when all He and H atoms are implanted as substitutional impurities. The resulting evolution in all species populations is qualitatively similar to that obtained for the case just discussed above where all He and H were implanted as interstitials. The only notable difference is that the incubation doses for various defect clusters are lower than in the previous case. For example, accumulation of SIA loops starts at a dose of 0.0008 dpa (compared to 0.0016 dpa), I_n–H loops at 0.001 dpa (compared to 0.004 dpa), and V–H bubbles at 0.1 dpa (compared to 0.3 dpa). Thus, the main effect of implanting He and H in substitutional form is to accelerate the kinetics of defect accumulation compared to the case when all gas atoms are implanted as interstitials. The size distribution of the defect species at 1 dpa is also shown in Fig. 8.

Regarding vacancy clusters, the 'substitutional' case results in larger and more numerous clusters than the 'interstitial' one. However, in both cases, all vacancy clusters (including bubbles) remain small containing no more than 10 vacancies[4] even at the highest simulated dose of 1 dpa. For SIA loops the differences are more striking. Fig. 8 shows that 'substitutional' implantation results in a higher number density of smaller SIA clsuters (up to 8.5 nm), whereas 'interstitial' implantation leads to the growth of fewer but much larger loops (~15 nm).

To better understand why the kinetics of damage accumulation between the 'interstitial' and 'substitutional' simulations differ so significantly, it is useful to consider the fractions of the total numbers of inserted SIAs, vacancies, and gas atoms that are absorbed at sinks (dislocations and grain boundaries). These are plotted in Fig. 9 as a function of dose. Initially nearly all He and H atoms implanted as interstitials are absorbed at sinks. The absorbed fractions then steadily decrease for both subspecies due to concurrent reactions with the SIA loops that begin to grow at a dose of approximately 0.1 dpa.

When all He and H atoms are inserted in the form of substitutional impurities, the kinetics of V and SIA accumulation remain very similar to the 'interstitial' case. However in the 'substitutional' simulations, the implanted H atoms are observed to occasionally

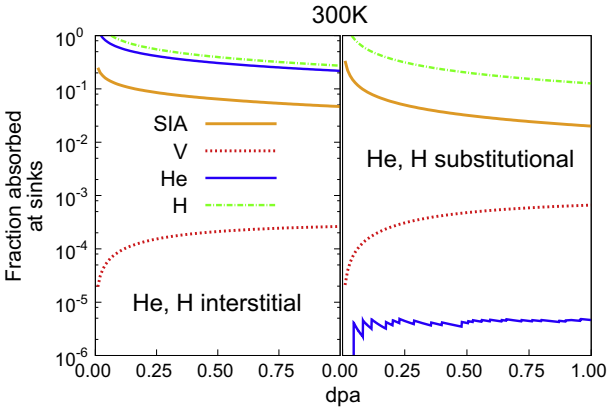

Fig. 9. Fraction of various defect subspecies absorbed by sinks relative to the total number of the same species inserted at 300 K, plotted as functions of dose. Vacancies are always absorbed faster than the other subspecies. Note the difference between the case when He is inserted substitutionally vs. when it is introduced interstitially.

dissociate from their host vacancies (E_b(H–V) = 0.57 eV) and become interstitial whereas, due to the higher V–He binding energy, He atoms implanted as substitutionals cannot escape their host vacancies and remain immobile. This makes He absorption at sinks exceedingly rare, and reduces the corresponding absorbed fraction to a negligible level, at which every absorption event manifests itself as a discrete jump in the curve in Fig. 9. At the same time, the rate of He absorption remains nearly constant over the entire dose interval.

4.4. Simulation of damage accumulation at 783 K

At a temperature of T = 783 K and 100% of gas atoms implanted as interstitial impurities, SCD simulations showed no discernible damage accumulated in the simulation volume up to the total displacement dose of 1 dpa. This is a direct consequence of the high diffusivities of interstitial H and He at this temperature, resulting in rapid absorption at sinks. This lack or scarcity of gas atoms reduces the probability for SIA and small SIA clusters to become mutually trapped with He and H so that they too are readily absorbed at sinks. For their part, small vacancy clusters generated directly in displacement cascades dissolve far too rapidly at this high temperature to allow for reactions with gas atoms in order to become thermally stable. The vacancies emitted in cluster

[4] V clusters are assumed to grow three-dimensionally as $r_n = \left(\frac{3n\Omega_a}{4\pi}\right)^{\frac{1}{3}}$.

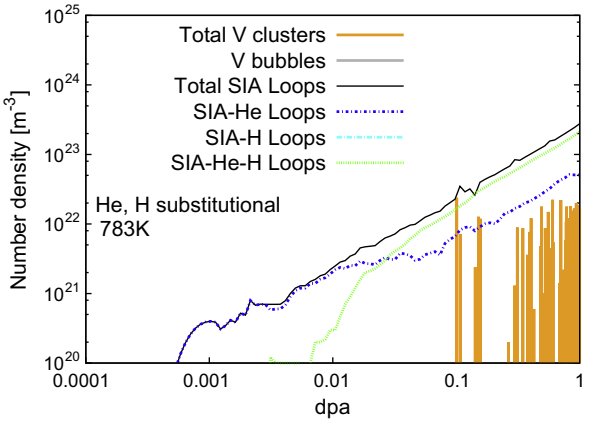

Fig. 10. Accumulation of defect species as a function of dose at 783 K for the case when He and H are implanted as substitutional atoms.

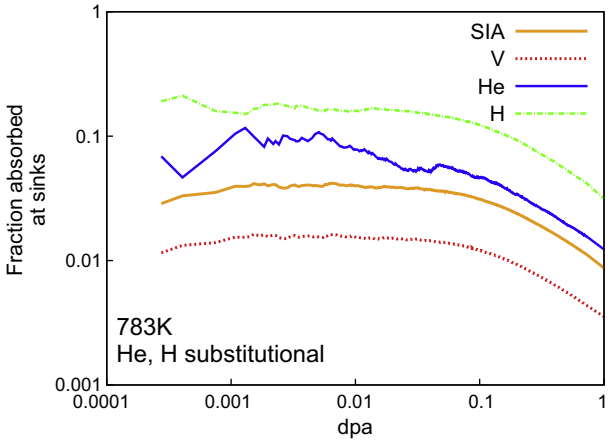

Fig. 12. Fractions of defects absorbed at sinks as a function of dose. All fractions decrease with dose as more SIA loops accumulate at doses >0.01 dpa.

dissociation reactions also have high diffusivity and quickly reach sinks themselves. Thus, under these irradiation conditions and up to a dose of 1 dpa, all defect species, whether produced in collision cascades or implanted, get absorbed at sinks. Although the possibility that loops and bubbles can nucleate at doses higher than 1 dpa exists, the difference with the low temperature simulations discussed above is striking.

By contrast, when implanted as substitutionals, He atoms are unable to dissociate from their host vacancies even at this high temperature. Trapping of He in substitutional form enhances their retention sufficiently for mobile SIA clusters to find them and form sessile clusters. As Fig. 10 shows, this occurs early, at a dose of 6.0×10^{-4} dpa. From that moment on, the number density of SIA clusters gradually increases. Because the binding energy of a substitutional H to its vacancy is much lower (0.57 eV, cf. Table 3), the as-implanted H–V clusters dissociate relatively quickly at this temperature releasing interstitial H that again is able to diffuse and reach sinks readily. Only after a substantial number of immobile SIA–He loops are accumulated (around 0.008 dpa) does the released interstitial H begin to react and become trapped. Notably, no I_n–H loops are formed without He mediation. Regarding vacancy clusters, small V clusters begin to form at a dose of about 0.1 dpa, only to dissolve shortly thereafter. In 0.3–1.0 dose interval, somewhat larger vacancy clusters appear sporadically, yet no gas bubbles are observed even at 1 dpa suggesting that the actual incubation dose is above the end dose of our SCD simulation.

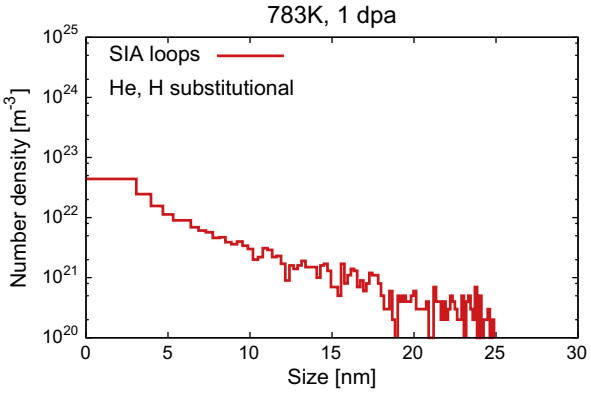

Fig. 11. SIA-loop size distributions at 783 K and 1 dpa for the cases where all He and H are inserted as substitutional impurities. No vacancy clusters (including bubbles) accumulate up to 1 dpa.

The size distribution of SIA loops at 1 dpa of irradiation dose is given in Fig. 11. Since all cascade-generated vacancy clusters dissociate rapidly and most of the released vacancies are rapidly absorbed at sinks, recombination with SIAs is limited. Under these circumstances, SIA loops, once formed, can grow to relatively large sizes—up to 25 nm in diameter, *i.e.* much larger than those observed during room temperature simulations in Section 4.3. Typically, loops with this size are decorated with approximately 10 He atoms and 60 H atoms.

Confirming the just described kinetic scenario, Fig. 12 shows the fractions of various defects that are directly absorbed at sinks, plotted as functions of dose. H atoms reach sinks as interstitials, after dissociating from their vacant site, resulting in a relatively smooth sink absorption evolution. Conversely, just as in the 300 K case, substitutional He migrates to sinks mostly by associating first with a free vacancy and then diffusing as a part of a He–V_2 cluster with lower mobility.

5. Discussion and conclusions

The main purpose of this paper was to describe how to recast existing ODE-RT models into Gillespie's stochastic simulation algorithm. Within the mean-field rate theory formulation for calculations of damage accumulation kinetics in irradiated materials, a number of numerical and physical issues are dealt with more consistently and/or conveniently within the SCD framework than in the standard ODE-based implementations. The key potential advantage over the ODE-RT is that the computational cost of SCD simulations is defined principally by the size of simulation volume. In contrast, in the ODE-RT the cost is defined mostly by the resolution of the ODE grid and, if a multi-species defect population is of interest, by the dimensionality of the cluster size space. In the latter case, computational complexity scales exponentially with the number of size dimensions, leading to *combinatorial explosion*, *i.e.* too many equations to solve. This situation is not unfamiliar in computational sciences, *e.g.* numerical evaluation of multi-dimensional integrals meets a similar computational challenge. The solution originally proposed by Gillespie in the context of chemical reaction networks [18] draws on the general strength of the Monte Carlo method, in which, rather than computing the integrand on every grid point, the integral is estimated by averaging random samples of the integrand. Now widely recognized and rigorously justified mathematically, a key advantage of the Monte Carlo method is that such random sampling does not have to be dense for computing the integral to an acceptable accuracy. Likewise in

SCD: accurate predictions of damage accumulation can be obtained by sparse random sampling of the evolving defect cluster populations.

Although the need and the ability to define a finite simulation volume may at first appear to be purely numerical concerns, stochastic finite-volume variations in defect species populations reflect real physics that are accounted for in SCD. Simulation volumes should be selected on the basis of a compromise between the computational cost of SCD simulations and the accuracy of their predictions. The danger of selecting too small a volume is that it may not be representative of the initial and/or evolving defect populations. We have already noted one such consideration—the diffusion lengths of mobile species—that has a bearing on volume selection. There can be other relevant but, perhaps, more subtle concerns affecting practical selection of V. The ability to control simulation volumes may also prove useful for a parallel implementation of the SCD method: partitioning of a large cluster population (in a large volume) into smaller sub-populations (each in a smaller sub-volume) offers a viable route to an efficient parallel SCD.

Although several workers have accounted for various aspects of cascade production and cluster migration fluctuations in RT [59–62], as an intrinsically stochastic technique, SCD is better suited than ODE-RT to deal with the probabilistic aspects of irradiation damage. Furthermore, the persistent issue of species non-conservation never arises in SCD because the cluster species populations are integer valued. For the same reason, there is no size distribution tails with which to be concerned in SCD.[5] In fact, the SCD method is remarkably close in its spirit to kMC: the only but essential difference between kMC and SCD is that the latter is a mean-field method and does not resolve the spatial positions of the cluster species. This close affinity of SCD and kMC opens the door to direct comparisons between the two methods on identical reaction–diffusion models, and may prove useful for the development of both approaches.

Notwithstanding these advantageous characteristics of the SCD method, it is also important to recognize that, at present, traditional ODE-RT implementations are much more efficient computationally for most material models currently in the literature. For example, it takes just minutes to integrate the ODEs representing the simple mean-field model in Ref.[9] (see Fig. 3 in Section 3) to a total damage dose of 0.01 dpa, whereas it has taken us several hours to reach the same dose in the SCD. The situation changes for the few known models with two-dimensional cluster size populations [14,35], where both ODE-RT and SCD may take hours to reach the same time scale (see Fig. 4). However, for models with three or more size attributes, the computational cost of SCD simulations increases only modestly, whereas ODE-RT calculations on the same models may well become prohibitive owing to combinatorial explosion.

At present, it is premature to make direct comparisons between standard ODE-RT and SCD in terms of computational efficiency. This is because over the history of the method and its applications, ODE-RT practitioners have accumulated a wealth of experience that has enabled them to enhance the method's computational efficiency, *e.g.* by taking advantage of state-of-the-art stiff ODE solvers [35]. In contrast, the proof-of-principle SCD implementation presented here is far from optimal. We expect the SCD method to benefit from numerical algorithms developed for computational chemistry and biology applications that substantially increase the efficiency of the SSA. Indeed, we are currently exploring the potential of the so-called *tau-leaping* [63], and *second-reaction* [64] methods, as well as several other stochastic algorithms to accelerate SCD simulations of irradiated materials.

In this paper, we have presented the first stochastic implementation of the rate theory approach: the *stochastic cluster dynamics* method. In order to verify our approach, we have applied it first to two different material rate models available in the literature. Then, inspired by the recent observations of enhanced swelling in triple-beam irradiation experiments of bcc materials, we have developed a new material rate model that explicitly considers complex defect species containing vacancies or SIAs, and He and H atoms. The cluster size space of this model is three-dimensional and provides a relevant framework for testing the new method. Four SCD simulations have been performed at two different temperatures, 300 and 783 K, using two distinctly different forms of the implantation source term. The simulations reveal multi-stage kinetics of damage accumulation at 300 K, and suggest that, at 783 K, the incubation dose for gas bubble nucleation exceeds the maximum dose of 1 dpa reached in the calculations. Our preliminary results demonstrate the potential of the new SCD method to model complex multi-stage kinetics of damage accumulation in materials containing defect clusters made up of constituent defects of multiple types. Our primary goal for further SCD method development is to enhance its computational efficiency in order to be able to model the radiation damage kinetics in more realistically complex materials and with ever increasing physical fidelity. We emphasize that, while pertinent and interesting, we are not yet in a position, and it is not the objective of this paper, to compare the experiments by Tanaka et al. [13] and our simulations. More work is indeed needed to increase the fidelity of our model by enriching it with more relevant kinetic and physical mechanisms.

Acknowledgments

This work was performed under the auspices of the US Department of Energy by Lawrence Livermore National Laboratory under Contract DE-AC52-07NA27344. We specifically acknowledge support from the Laboratory Directed Research and Development Program under Project 09-SI-003. Fruitful discussions with W. Wolfer are gratefully acknowledged. VVB wishes to thank F. Willaime and the SRMP group for their warm hospitality during his sabbatical stay at CEA Saclay where initial ideas for this work were conceived. VVB especially acknowledges fruitful discussions with A. Barbu, M. Athenes and T. Jourdan (all at CEA-Saclay). Early trial implementations of the SCD method are due to Solene LeBourdiec (EDF) and Tuan Hoang (UC Berkeley) whose contributions both authors gratefully acknowledge.

References

[1] A.D. Brailsford, R. Bullough, Journal of Nuclear Materials 44 (1972) 121.
[2] B.T. Kelly, Carbon 14 (1976) 239.
[3] L.K. Mansur, M.H. Yoo, Journal of Nuclear Materials 85–86 (1979) 523.
[4] N.M. Ghoniem, Radiation Effects & Defects in Solids 148 (1999) 269.
[5] G.R. Odette, B.D. Wirth, D.J. Bacon, N.M. Ghoniem, MRS Bulletin (2001) 176.
[6] C. Domain, C.S. Becquart, L. Malerba, Journal of Nuclear Materials 335 (2004) 121.
[7] M.J. Caturla, N. Soneda, T. Diaz de la Rubia, M. Fluss, Journal of Nuclear Materials 351 (2006) 78.
[8] A. Donev, V.V. Bulatov, T. Oppelstrup, G.H. Gilmer, B. Sadigh, M.H. Kalos, Journal of Computational Physics 229 (2010) 3214.
[9] R.E. Stoller, S.I. Golubov, C. Domain, C.S. Becquart, Journal of Nuclear Materials 382 (2008) 77.
[10] K. Tapasa, A.V. Barashev, D.J. Bacon, Y.N. Osetsky, Acta Materialia 55 (2007) 1.
[11] G.R. Odette, G.E. Lucas, JOM 53 (2001) 18.
[12] L.M. Wang, R.A. Dodd, G.L. Kulcinski, Journal of Nuclear Materials 141–142 (1986) 713.
[13] T. Tanaka, K. Oka, S. Ohnuki, S. Yamashita, T. Suda, S. Watanabe, E. Wakai, Journal of Nuclear Materials 329–333 (2004) 294.
[14] S.I. Golubov, R.E. Stoller, S.J. Zinkle, A.M. Ovcharenko, Journal of Nuclear Materials 361 (2007) 149.
[15] M. Kiritani, Journal of the Physics Society of Japan 35 (1973) 95.

[5] Parenthetically, elements of the SSA were first employed for irradiation damage simulations by Surh and Wolfer [35], but only as a way to handle distribution tails. The bulk of the species population was still treated within standard ODE-RT with all of its numerous ODEs to solve.

[16] S.I. Golubov, A.M. Ovcharenko, A.V. Barashev, B.N. Singh, Philosophical Magazine A 81 (2001) 643.
[17] M. Koiwa, Journal of the Physics Society of Japan 37 (1974) 1532.
[18] D.T. Gillespie, Journal of Computational Physics 22 (1976) 403.
[19] H. Kitano, Nature 420 (2002) 206.
[20] D.T. Gillespie, Journal of Physical Chemistry 81 (1977) 2340.
[21] F. Leyvraz, S. Redner, Physical Review Letters 66 (1991) 2168.
[22] A.B. Bortz, M.H. Kalos, J.L. Lebowitz, Journal Computational Physics 17 (1975) 10.
[23] A.F. Voter, Introduction to the kinetic Monte Carlo method, in: K.E. Sickafus, E.A. Kotomin (Eds.), Radiation Effects in Solids, Springer, The Netherlands, 2005.
[24] N.M. Ghoniem, Journal of Nuclear Materials 179–181 (1991) 99.
[25] S. Redner, A Guide to First-passage Processes, Cambridge University Press, 2001, p. 214.
[26] M. von Smoluchowski, Zeitschrift fur Physik 17 (1916) 557.
[27] U. Gösele, A. Seeger, Philosophical Magazine 34 (1976) 177.
[28] S.L. Hardt, Biophysical Chemistry 10 (1979) 239.
[29] M. Rathinam, L.R. Pretzold, Y. Cao, D. Gillespie, Journal of Chemical Physics 119 (2003) 12784.
[30] http://www.uthash.sourceforge.net.
[31] A. Barbu, C.S. Becquart, J.L. Bocquet, J. Dalla Torre, C. Domain, Philosophical Magazine 85 (2005) 541.
[32] A. Barbu, Private communication (2010).
[33] R. Bullough, M.R. Hayns, M.H. Wood, Journal of Nuclear Materials 90 (1980) 44.
[34] A.D. Brailsford, R. Bullough, Philosophical Transactions of the Royal Society of London Series A 302 (1981) 87.
[35] M.P. Surh, J.B. Sturgeon, W.G. Wolfer, Journal of Nuclear Materials 378 (2008) 86.
[36] S. Hamada, Y.C. Zhang, Y. Miwa, D. Yamaki, Radiation Physics and Chemistry 50 (1997) 555.
[37] N. Sekimura, T. Iwai, Y. Arai, S. Yonamine, A. Naito, Y. Miwa, S. Hamada, Journal of Nuclear Materials 283–287 (2000) 224.
[38] http://www.srim.org.
[39] L. Malerba, Journal of Nuclear Materials 351 (2006) 28.
[40] L. Malerba, M.C. Marinica, N. Anento, C. Björkas, H. Nguyen, C. Domain, F. Djurabekova, P. Olsson, K. Nordlund, A. Serra, D. Terentyev, F. Willaime, C.S. Becquart, Journal of Nuclear Materials 406 (2010) 19.
[41] N. Anento, A. Serra, Yu N. Osetsky, Modelling and Simulation in Materials Science and Engineering 18 (2010) 025008.
[42] J. Marian, B.D. Wirth, A. Caro, B. Sadigh, G.R. Odette, J.M. Perlado, T. Diaz de la Rubia, Physical Review B 65 (2002) 144102.
[43] M.I. Mendelev, Y. Mishin, Physical Review B 80 (2009) 144111.
[44] F. Djurabekova, L. Malerba, R.C. Pasianot, P. Olsson, K. Nordlund, Philosophical Magazine 90 (2010) 2585.
[45] C.-C. Fu, F. Willaime, Physical Review B 72 (2005) 064117.
[46] D. Terentyev, N. Juslin, K. Nordlund, N. Sandberg, Journal of Applied Physics 105 (2009) 103509.
[47] D.M. Stewart, Yu N. Osetsky, R.E. Stoller, S.I. Golubov, T. Seletskaia, P.J. Kamenski, Philosophical Magazine 90 (2010) 935.
[48] D.E. Jiang, E.A. Carter, Physical Review B 70 (2004) 064102.
[49] C.-C. Fu, J. Dalla Torre, F. Willaime, J.-L. Bocquet, A. Barbu, Nature Materials 4 (2005) 68.
[50] N. Soneda, T. Diaz de la Rubia, Philosophical Magazine A 81 (2001) 331.
[51] W.A. Counts, C. Wolverton, R. Gibala, Acta Materialia 58 (2010) 4730.
[52] P.R. Monasterio, T.T. Lau, S. Yip, K.J. Van Vliet, Physical Review Letters 103 (2009) 085501.
[53] V.V. Kirsanov, M.V. Musina, V.V. Rybin, Journal of Nuclear Materials 191–194 (1992) 1318.
[54] L. Ventelon, B.D. Wirth, C. Domain, Journal of Nuclear Materials 351 (2006) 119.
[55] G. Lucas, R. Schäublin, Journal of Physics: Condensed Matter 20 (2008) 415206.
[56] F.A. Garner, E.P. Simonen, B.M. Oliver, L.R. Greenwood, M.L. Grossbeck, W.G. Wolfer, P.M. Scott, Journal of Nuclear Materials 356 (2006) 122.
[57] P. Erhart, J. Marian, Journal of Nuclear Materials (2011), doi:10.1016/j.jnucmat.2011.05.017.
[58] L.K. Mansur, Mechanisms and kinetics of radiation effects in metals and alloys, in: G.R. Freeman (Ed.), Kinetics of Non-Homogeneous Processes, Wiley Interscience, New York, 1987, pp. 377–463.
[59] K. Kitajima, Journal of Nuclear Materials 133–134 (1985) 64.
[60] P. Chou, N.M. Ghoniem, Journal of Nuclear Materials 137 (1985) 63.
[61] N.M. Ghoniem, Physical Review B 39 (1989) 11810.
[62] A.A. Semenov, C.H. Woo, Journal of Nuclear Materials 205 (1993) 74.
[63] A. Chatterjee, D.G. Vlachos, M.A. Katsoulakis, Journal of Chemical Physics 122 (2005) 024112.
[64] M.A. Gibson, J. Bruck, Journal of Physical Chemistry A 104 (2000) 1876.